INSTITUTE OF PHYSICS PUBLISHING SMART MATERIALS AND STRUCTURES
Smart Mater. Struct. **14** (2005) 989–1000 doi:10.1088/0964-1726/14/5/037

Damage detection in nonlinear systems using system augmentation and generalized minimum rank perturbation theory

Kiran D'Souza and Bogdan I Epureanu[1]

Department of Mechanical Engineering, University of Michigan, Ann Arbor, MI 48109-2125, USA

E-mail: epureanu@umich.edu

Received 27 July 2004, in final form 21 March 2005
Published 2 September 2005
Online at stacks.iop.org/SMS/14/989

Abstract
A damage detection method is developed for nonlinear systems using model updating. The method uses a nonlinear discrete model of the system and the form of the nonlinearities to create an augmented linear model of the system. A modal analysis technique that uses forcing that is known but not prescribed is then used to solve for the modal properties of the augmented linear system after the onset of damage. Due to the specialized form of the augmentation, nonlinear damage causes asymmetrical damage in the updated matrices. Minimum rank perturbation theory is generalized so that it may be applied to the augmented system and can handle these asymmetrical damage scenarios. The method is demonstrated using numerical data from several nonlinear mass–spring systems.

1. Introduction

Health monitoring and online damage detection of structural systems is of growing importance in many fields. The aerospace industry is one of the fields where these methods are applied. Many current structural damage detection techniques are focused on identifying changes in the linear system behavior [10] and employ linear methods based on changes in the natural frequencies and mode shapes [26]. Also, system identification [1, 12, 21, 24, 30] and generic (and not necessarily physical) models such as neural networks [2, 23, 36] are used. With the increasing demand for safe space technology, the various structural systems that compose air and space vehicles must be monitored for safety and reliability. Hence, the current most common methods of visual inspection and time-based maintenance will be upgraded to online monitoring of the integrity of the vehicle and condition-based maintenance.

The field of nonlinear experimental modal analysis is an active area of research which plays an important role in nonlinear vibration-based damage detection. Worden and Tomlinson [33] separate the research in this field into three main areas. The first area uses the basic theory and philosophy of linear modal analysis by characterizing the nonlinear system in a way such that the amplitude invariance is lost. The study of the frequency response function's (FRF) distortion was one of the early studies in this area by Ewins [9]. The second area consists of extending the linear approach of modal analysis to encompass quantities that are amplitude invariants of nonlinear systems. For example, Gifford [14] develops a technique in this area which is based on Volterra series [25] and obtains the linear parameters from a nonlinear optimization step and the nonlinear parameters from a linear least squares analysis of higher-order FRFs (HFRFs). The third area of the study of nonlinearity in modal analysis requires the discarding of the linear theory and the creation of new theories to address the nonlinearity directly, such as nonlinear normal modes [20, 22, 27, 28] and center manifold theory [31, 34].

The field of linear modal analysis is much more developed than its nonlinear counterpart. Linear techniques based on single input single output, single input multiple output, and multiple input multiple output (MIMO) approaches are

[1] Author to whom any correspondence should be addressed.

available. These techniques are developed for both time and frequency domains. The time-based MIMO methods have several different characteristics which were surveyed by Yang *et al* [35]. The poly-reference complex exponential [32], eigensystem realization algorithm [17] and Ibrahim time domain [29] methods find the modal properties using impulse or free responses of the system. The auto-regressive moving average vector [37] and direct system parameter identification (DSPI) [19] both use the response of systems forced by natural excitations to determine modal properties.

Using modal analysis to obtain the mode shapes and natural frequencies is the first step in many structural health monitoring approaches. The modal properties are then used in a damage detection algorithm. The linear nondestructive evaluation field has been developed greatly and includes four general categories: optimal matrix updates, sensitivity methods, eigenstructure assignment techniques, and minimum rank perturbation methods (for a review, see the papers by Ibrahim [16] and Heylen [15]).

In this work an algorithm for analyzing a nonlinear system as an augmented linear system is presented. This allows for the much better developed areas of linear modal analysis and linear damage detection to be exploited. A key feature of the augmentation requires the modal analysis technique used to work with a forcing that is known but not prescribed. A MIMO technique such as DSPI [19] that uses natural excitations of the system as forcing is the technique used in this paper to identify the modal properties of the augmented system. Nonetheless, other techniques may be used as well. Next, the modal properties of the augmented system are used in conjunction with a novel generalized minimum rank perturbation theory (GMRPT) to detect the location and extent of damage in nonlinear systems. The proposed GMRPT is designed to account for nonlinearities, and is inspired from a linear damage detection technique employing minimum rank perturbation theory (MRPT) [38–41]. A key characteristic of the proposed augmentation is that the nonlinear damage is manifested in an asymmetrical fashion in the system matrices. A formulation of GMRPT is proposed to handle cases of asymmetric damage and nonlinear systems.

To demonstrate the proposed approach, the method is applied to several nonlinear mass–spring systems. The effectiveness of the augmentation and the GMRPT are demonstrated by numerical experiments. Also, the influence of measurement noise and of inaccuracies in modal parameters is analyzed.

2. General methodology

In this section, the procedure for detecting the location and extent of damage in nonlinear systems using linear theories is demonstrated. First, the modeling of the nonlinear system by an augmented linear one is introduced. Then, a means to solve the eigenvalue problem for the augmented system using DSPI [19] is detailed. Next, GMRPT is developed for damage that is not symmetric, which is a characteristic of the augmented system.

2.1. System augmentation for modeling nonlinear systems

In this section, a method to model a nonlinear system by an augmented linear system is presented. Consider a nonlinear system (characterized by a coordinate vector $\mathbf{x}$ and forced by an external excitation $\mathbf{g}(t)$) expressed as

$$\mathbf{M}\ddot{\mathbf{x}} + \mathbf{D}\dot{\mathbf{x}} + \mathbf{K}\mathbf{x} + \mathbf{f}(\mathbf{x}, \dot{\mathbf{x}}, \ddot{\mathbf{x}}) = \mathbf{g}(t), \qquad \text{or}$$
$$\begin{bmatrix} \mathbf{M} & \mathbf{0} \\ \mathbf{0} & \mathbf{I} \end{bmatrix} \begin{bmatrix} \ddot{\mathbf{x}} \\ \dot{\mathbf{x}} \end{bmatrix} + \begin{bmatrix} \mathbf{D} & \mathbf{K} \\ -\mathbf{I} & \mathbf{0} \end{bmatrix} \begin{bmatrix} \dot{\mathbf{x}} \\ \mathbf{x} \end{bmatrix} + \begin{bmatrix} \mathbf{f}(\mathbf{x}, \dot{\mathbf{x}}, \ddot{\mathbf{x}}) \\ \mathbf{0} \end{bmatrix} = \begin{bmatrix} \mathbf{g}(t) \\ \mathbf{0} \end{bmatrix}, \tag{1}$$

where $\mathbf{M}$, $\mathbf{D}$, and $\mathbf{K}$ are the mass, damping and stiffness matrices and $\mathbf{f}$ is a nonlinear function. Equation (1) can be rewritten as

$$\mathbf{M}\ddot{\mathbf{x}} + \mathbf{D}\dot{\mathbf{x}} + \mathbf{K}\mathbf{x} + \mathbf{N}\mathbf{y} = \mathbf{g}(t), \qquad \text{or}$$
$$\begin{bmatrix} \mathbf{M} & \mathbf{0} & \mathbf{0} & \mathbf{0} \\ \mathbf{0} & \mathbf{I} & \mathbf{0} & \mathbf{0} \\ \mathbf{0} & \mathbf{0} & \mathbf{I} & \mathbf{0} \\ \mathbf{0} & \mathbf{0} & \mathbf{0} & \mathbf{I} \end{bmatrix} \begin{bmatrix} \ddot{\mathbf{x}} \\ \dot{\mathbf{x}} \\ \ddot{\mathbf{y}} \\ \dot{\mathbf{y}} \end{bmatrix} + \begin{bmatrix} \mathbf{D} & \mathbf{K} & \mathbf{0} & \mathbf{N} \\ -\mathbf{I} & \mathbf{0} & \mathbf{0} & \mathbf{0} \\ \mathbf{0} & \mathbf{N}^{\mathrm{T}} & \mathbf{0} & 2\mathbf{I} \\ \mathbf{0} & \mathbf{0} & -\mathbf{I} & \mathbf{0} \end{bmatrix} \begin{bmatrix} \dot{\mathbf{x}} \\ \mathbf{x} \\ \dot{\mathbf{y}} \\ \mathbf{y} \end{bmatrix} = \begin{bmatrix} \mathbf{g}(t) \\ \mathbf{0} \\ \mathbf{h}(t) \\ \mathbf{0} \end{bmatrix}, \tag{2}$$

where $\mathbf{N}$ is a constant matrix, and $\mathbf{y}$ contains nonlinear terms of the form $(\mathrm{d}^m x_i/\mathrm{d}t^m)^p(\mathrm{d}^n x_j/\mathrm{d}t^n)^q$, with integer m, n, p, q. The function $\mathbf{h}(t)$ in equation (2) is introduced to preserve most of the properties of the matrices in equation (1). The augmentation is expressed such that it matches the form used in examples later in this paper. However, the system can be augmented differently to optimally suit various applications. Equation (2) is the augmented linear model of the nonlinear system for which the eigenvalue problem must be solved.

2.2. Eigenvalue problem for augmented systems

To use the augmented model given in the previous section, a modal analysis technique which uses an excitation that is known but not prescribed is needed. An example of a modal analysis technique that meets these requirements is DSPI, and it is also the technique used to generate data for this paper. DSPI enables one to determine the mode shapes and natural frequencies of the system when the displacement of the degrees of freedom ($\mathbf{x}(t)$ and $\mathbf{y}(t)$) and the forcing ($\mathbf{g}(t)$ and $\mathbf{h}(t)$) are known.

An example of implementation of the proposed approach is to measure the displacement vector $\mathbf{x}(t)$ and the forcing vector $\mathbf{g}(t)$. The vector $\mathbf{y}(t)$ may then be computed from $\mathbf{x}(t)$, and the vector $\mathbf{h}(t)$ may be calculated to satisfy equation (2). The requirement of the modal analysis technique to use a known but not prescribed forcing stems from the known forcing $\mathbf{h}(t)$.

A consequence of the form of the augmentation is the inability for damage to be modeled in the augmentation. This means that if damage occurs in $\mathbf{N}$ it will only be reflected in the linear portion and not the augmented portion of the system. The end result is that, when using this augmentation, nonlinear damage causes asymmetrical changes in the system matrices.

2.3. Generalized minimum rank perturbation theory

In this section, MRPT is generalized to handle cases where linear and nonlinear damage is present and the damage is not necessarily symmetric. First, the location algorithm is presented, and then the modified extent calculation is formulated.

2.3.1. Identification of damage location. The damage location algorithm for GMRPT follows closely that of MRPT [38–41] except for the addition of several equations that are used in the identification of the damage extent. It is assumed that a discrete, n-degree of freedom (e.g. finite element) model exists for the healthy system, and may be expressed as

$$\mathbf{M}\ddot{\mathbf{w}} + \mathbf{D}\dot{\mathbf{w}} + \mathbf{K}\mathbf{w} = \mathbf{0}, \tag{3}$$

where $\mathbf{M}$, $\mathbf{D}$ and $\mathbf{K}$ are $n \times n$ mass, damping and stiffness matrices, and $\mathbf{w}$ is an $n \times 1$ vector of displacements. The eigenvalue problem of equation (3) (i.e. λ-equation) can be written in second-order form as

$$\begin{aligned} \left(\lambda_{\mathrm{h}i}^2\mathbf{M} + \lambda_{\mathrm{h}i}\mathbf{D} + \mathbf{K}\right)\mathbf{v}_{\mathrm{h}i} &= \mathbf{0}, \\ \mathbf{u}_{\mathrm{h}i}^{\mathrm{T}}\left(\lambda_{\mathrm{h}i}^2\mathbf{M} + \lambda_{\mathrm{h}i}\mathbf{D} + \mathbf{K}\right) &= \mathbf{0}, \end{aligned} \tag{4}$$

where $\lambda_{\mathrm{h}i}$, $\mathbf{v}_{\mathrm{h}i}$ and $\mathbf{u}_{\mathrm{h}i}$ denote the ith eigenvalue, ith right eigenvector, and ith left eigenvector of the healthy structure. Next, consider that the ith eigenvalue $\lambda_{\mathrm{d}i}$, ith right eigenvector $\mathbf{v}_{\mathrm{d}i}$, and ith left eigenvector $\mathbf{u}_{\mathrm{d}i}$ of the damaged structure are measured (e.g. through modal analysis and DSPI). Let $\Delta\mathbf{M}$, $\Delta\mathbf{D}$ and $\Delta\mathbf{K}$ be the exact perturbation matrices that reflect the nature of the structural damage. Thus, the exact perturbation matrices are sparse matrices with the nonzero elements reflecting the presence of the damage. The λ-equation for the damaged structure may be expressed as

$$\begin{aligned} \left[\lambda_{\mathrm{d}i}^2(\mathbf{M} - \Delta\mathbf{M}) + \lambda_{\mathrm{d}i}(\mathbf{D} - \Delta\mathbf{D}) + (\mathbf{K} - \Delta\mathbf{K})\right]\mathbf{v}_{\mathrm{d}i} &= \mathbf{0}, \\ \mathbf{u}_{\mathrm{d}i}^{\mathrm{T}}\left[\lambda_{\mathrm{d}i}^2(\mathbf{M} - \Delta\mathbf{M}) + \lambda_{\mathrm{d}i}(\mathbf{D} - \Delta\mathbf{D}) + (\mathbf{K} - \Delta\mathbf{K})\right] &= \mathbf{0}. \end{aligned} \tag{5}$$

Although only p of the n eigenvalues/eigenvectors are assumed measured (with $p \ll n$), these equations hold for any particular eigenvalue and eigenvector of the damaged structure because the perturbation matrices are assumed to be exact. Grouping all perturbation matrices on the right-hand side defines two damage vectors $\mathbf{d}_i$ and $\mathbf{c}_i$ as

$$\mathbf{d}_i \equiv \mathbf{Z}_{\mathrm{d}i}\mathbf{v}_{\mathrm{d}i} = \left(\lambda_{\mathrm{d}i}^2\Delta\mathbf{M} + \lambda_{\mathrm{d}i}\Delta\mathbf{D} + \Delta\mathbf{K}\right)\mathbf{v}_{\mathrm{d}i}, \tag{6}$$

$$\mathbf{c}_i^{\mathrm{T}} \equiv \mathbf{u}_{\mathrm{d}i}^{\mathrm{T}}\mathbf{Z}_{\mathrm{d}i} = \mathbf{u}_{\mathrm{d}i}^{\mathrm{T}}\left(\lambda_{\mathrm{d}i}^2\Delta\mathbf{M} + \lambda_{\mathrm{d}i}\Delta\mathbf{D} + \Delta\mathbf{K}\right), \tag{7}$$

$$\mathbf{Z}_{\mathrm{d}i} \equiv \lambda_{\mathrm{d}i}^2\mathbf{M} + \lambda_{\mathrm{d}i}\mathbf{D} + \mathbf{K}. \tag{8}$$

A composite damage vector may be defined from the multiple measured modes as

$$\mathbf{d} = \frac{1}{p}\sum_{i=1}^{p}\frac{\mathbf{d}_i}{\|\mathbf{v}_{\mathrm{d}i}\|}. \tag{9}$$

Also, Zimmerman [38–41] developed an alternative view of the state of damage where equation (6) can be rewritten as

$$d_i^j \equiv \mathbf{z}_{\mathrm{d}i}^j\mathbf{v}_{\mathrm{d}i} = \|\mathbf{z}_{\mathrm{d}i}^j\|\|\mathbf{v}_{\mathrm{d}i}\|\cos(\theta_i^j), \tag{10}$$

where d_i^j is the jth component (i.e. jth degree of freedom, DOF) of the ith damage vector, $\mathbf{z}_{\mathrm{d}i}^j$ is the jth row of the matrix $\mathbf{Z}_{\mathrm{d}i}$, and θ_i^j is the angle between the vectors $\mathbf{z}_{\mathrm{d}i}^j$ and $\mathbf{v}_{\mathrm{d}i}$. A damage detector α_i^j may be calculated from θ_i^j, where

$$\alpha_i^j = \theta_i^j\left(\frac{180^\circ}{\pi}\right) - 90^\circ. \tag{11}$$

A composite damage vector γ may be defined from the multiple measured modes as

$$\gamma_j = \frac{1}{p}\sum_{i=1}^{p}|\alpha_i^j|. \tag{12}$$

2.3.2. Identification of damage extent. Often it is of interest to determine the extent of the structural damage in addition to its location. Due to the nature of the augmentation, the perturbation matrices, $\Delta\mathbf{M}$, $\Delta\mathbf{D}$ and $\Delta\mathbf{K}$, may not be symmetric. For simplicity, in the following it is assumed that the structure under consideration is undamped (and that both $\mathbf{M}$ and $\mathbf{K}$ are symmetric). Nonetheless, the presence of damping can be included with little change to the proposed methodology. Furthermore, it is assumed the effect of the damage on the mass is negligible. Equations (6) and (7) can be rewritten with these assumptions as

$$\begin{aligned} \left(\lambda_{\mathrm{d}i}^2\mathbf{M} + \mathbf{K}\right)\mathbf{v}_{\mathrm{d}i} &= \Delta\mathbf{K}\mathbf{v}_{\mathrm{d}i} \equiv \mathbf{d}_i, \\ \mathbf{u}_{\mathrm{d}i}^{\mathrm{T}}\left(\lambda_{\mathrm{d}i}^2\mathbf{M} + \mathbf{K}\right) &= \mathbf{u}_{\mathrm{d}i}^{\mathrm{T}}\Delta\mathbf{K} \equiv \mathbf{c}_i^{\mathrm{T}}, \end{aligned} \tag{13}$$

where $i = 1, \ldots, p$ as it is assumed that only p damaged eigenvalues and eigenvectors are measured. These equations can be rewritten in matrix form as

$$\begin{aligned} \mathbf{M}\mathbf{V}_{\mathrm{d}}\mathbf{\Lambda}_{\mathrm{d}} + \mathbf{K}\mathbf{V}_{\mathrm{d}} &= \Delta\mathbf{K}\mathbf{V}_{\mathrm{d}} \equiv \mathbf{B}, \\ \mathbf{\Lambda}_{\mathrm{d}}\mathbf{U}_{\mathrm{d}}^{\mathrm{T}}\mathbf{M} + \mathbf{U}_{\mathrm{d}}^{\mathrm{T}}\mathbf{K} &= \mathbf{U}_{\mathrm{d}}^{\mathrm{T}}\Delta\mathbf{K} \equiv \mathbf{A}^{\mathrm{T}}, \end{aligned} \tag{14}$$

where

$$\begin{aligned} \mathbf{\Lambda}_{\mathrm{d}} &= \mathrm{diag}(\lambda_{\mathrm{d}1}^2, \lambda_{\mathrm{d}2}^2, \ldots, \lambda_{\mathrm{d}p}^2), \\ \mathbf{V}_{\mathrm{d}} &= [\mathbf{v}_{\mathrm{d}1}, \mathbf{v}_{\mathrm{d}2}, \ldots, \mathbf{v}_{\mathrm{d}p}], \\ \mathbf{B} &= [\mathbf{d}_1, \mathbf{d}_2, \ldots, \mathbf{d}_p], \\ \mathbf{U}_{\mathrm{d}}^{\mathrm{T}} &= [\mathbf{u}_{\mathrm{d}1}, \mathbf{u}_{\mathrm{d}2}, \ldots, \mathbf{u}_{\mathrm{d}p}]^{\mathrm{T}}, \\ \mathbf{A}^{\mathrm{T}} &= [\mathbf{c}_1, \mathbf{c}_2, \ldots, \mathbf{c}_p]^{\mathrm{T}}. \end{aligned} \tag{15}$$

The algorithm for identifying the damage extent is mathematically supported by the following.

Proposition. *Suppose that* $\mathbf{V}_{\mathrm{d}} \in \Re^{n\times p}$, $\mathbf{B} \in \Re^{n\times p}$ *and* $\mathbf{A} \in \Re^{n\times p}$ *are given, where* $p < n$ *and* $\mathrm{rank}(\mathbf{V}_{\mathrm{d}}) = \mathrm{rank}(\mathbf{B}) = \mathrm{rank}(\mathbf{A}) = p$. *Define* $\mathcal{K}$ *to be the set of matrices* $\Delta\mathbf{K}$ *in* $\Re^{n\times n}$ *that satisfies*

$$\Delta\mathbf{K}\mathbf{V}_{\mathrm{d}} = \mathbf{B}, \tag{16}$$

$$\mathbf{U}_{\mathrm{d}}^{\mathrm{T}}\Delta\mathbf{K} = \mathbf{A}^{\mathrm{T}}. \tag{17}$$

Then

(a) If the set $\mathcal{K}$ *is nonempty, then the minimum rank of any matrix* $\Delta\mathbf{K}$ *in* $\mathcal{K}$ *is* p. *Next, define* $\mathcal{K}^p$ *to be a subset of* $\mathcal{K}$ *comprised of all* $\Delta\mathbf{K}$ *such that* $\mathrm{rank}(\Delta\mathbf{K}) = p$.

(b) One member of $\mathcal{K}^p$ *is given by*

$$\Delta\mathbf{K}^p = \mathbf{B}\mathbf{H}\mathbf{A}^{\mathrm{T}} \qquad \textit{with } \mathbf{H} = \left(\mathbf{A}^{\mathrm{T}}\mathbf{V}_{\mathrm{d}}\right)^{-1}. \tag{18}$$

(c) The matrix defined by equation (18) is the unique member of $\mathcal{K}^p$.

To prove proposition (a), note that equations (16) and (17) are exactly satisfied if and only if range($\mathbf{B}$) and range($\mathbf{A}$)

are included in range($\Delta\mathbf{K}$). This implies that rank($\mathbf{B}$) = rank($\mathbf{A}$) = $p \leqslant$ rank($\Delta\mathbf{K}$). Hence, the minimum rank of $\Delta\mathbf{K}$ is p.

To prove proposition (b), assume that the expanded singular value decomposition of member j of $\mathcal{K}^p$, $\Delta\mathbf{K}^{p,j}$, to be of the form

$$\Delta\mathbf{K}^{p,j} = \mathbf{U}^j \boldsymbol{\Sigma}^j \mathbf{V}^{j\mathrm{T}}, \tag{19}$$

where

$$\mathbf{U}^j = \left[\mathbf{u}_1^j, \mathbf{u}_2^j, \ldots, \mathbf{u}_p^j\right],$$

$$\boldsymbol{\Sigma}^j = \mathrm{diag}\left(\sigma_1^j, \sigma_2^j, \ldots, \sigma_p^j\right),$$

$$\mathbf{V}^{j\mathrm{T}} = \left[\mathbf{v}_1^j, \mathbf{v}_2^j, \ldots, \mathbf{v}_p^j\right]^{\mathrm{T}},$$

where the superscript j indicates the jth family member, the vectors $\mathbf{u}_i^j$ are the left singular vectors, the vectors $\mathbf{v}_i^j$ are the right singular vectors, and the values σ_i^j are nonzero singular values of $\Delta\mathbf{K}^{p,j}$. In the expanded singular value decomposition, the singular vectors with indices from (p+1) to n are not shown in the factorization because they all correspond to zero singular values. For equations (16) and (17) to be satisfied, the range of $\mathbf{B}$ must equal the range of $\mathbf{U}^j$ and the range of $\mathbf{A}$ must equal the range of $\mathbf{V}^j$. Therefore, the matrices $\mathbf{B}$ and $\mathbf{U}^j$ can be related by an invertible $p \times p$ matrix $\mathbf{Q}^j$ as follows:

$$\mathbf{B} = \mathbf{U}^j \mathbf{Q}^j, \qquad \text{where } \mathbf{Q}^j = \boldsymbol{\Sigma}^j \mathbf{V}^{j\mathrm{T}} \mathbf{V}_\mathrm{d}. \tag{20}$$

Likewise, the matrices $\mathbf{A}$ and $\mathbf{V}^j$ can be related by an invertible $p \times p$ matrix $\mathbf{P}^j$ as follows:

$$\mathbf{A} = \mathbf{V}^j \mathbf{P}^j, \qquad \text{where } \mathbf{P}^j = \boldsymbol{\Sigma}^j \mathbf{U}^{j\mathrm{T}} \mathbf{U}_\mathrm{d}. \tag{21}$$

Substituting equations (20) and (21) into (19) yields

$$\Delta\mathbf{K}^{p,j} = \mathbf{B}\mathbf{Q}^{j-1}\boldsymbol{\Sigma}^j\mathbf{P}^{j-\mathrm{T}}\mathbf{A}^\mathrm{T} = \mathbf{B}\mathbf{H}^j\mathbf{A}^\mathrm{T}. \tag{22}$$

Thus, each family member is uniquely defined by the factorization of equation (22). Also, it is evident that $\mathbf{H}^j$ is of full rank because its inverse exists (and it is given by $\mathbf{P}^{j\mathrm{T}}\boldsymbol{\Sigma}^{j-1}\mathbf{Q}^j$).

Inspection of equation (22) reveals that the only unknown term in the factorization is $\mathbf{H}^j$. Equation (16) can be rewritten using the factorization of $\Delta\mathbf{K}^{p,j}$, defined by equation (22), as

$$\mathbf{B} = \Delta\mathbf{K}^{p,j}\mathbf{V}_\mathrm{d} = \left(\mathbf{B}\mathbf{H}^j\mathbf{A}^\mathrm{T}\right)\mathbf{V}_\mathrm{d} = \mathbf{B}\left(\mathbf{H}^j\mathbf{A}^\mathrm{T}\mathbf{V}_\mathrm{d}\right). \tag{23}$$

The equation above is satisfied if and only if $\mathbf{H}^j\mathbf{A}^\mathrm{T}\mathbf{V}_\mathrm{d} = \mathbf{I}$, where $\mathbf{I}$ is the $p \times p$ identity matrix. This holds because $\mathbf{B}$ is of full column rank. Thus, $\mathbf{H}^j$ is uniquely calculated to be

$$\mathbf{H}^j = \left(\mathbf{A}^\mathrm{T}\mathbf{V}_\mathrm{d}\right)^{-1}. \tag{24}$$

Hence, equation (18) holds as shown by equations (22) and (24).

The proof of proposition (c) follows immediately by inspecting the right-hand side of equation (24). Inspection reveals that $\mathbf{H}^j$ is the same for all members of $\mathcal{K}^p$. This fact, in conjunction with equation (22), leads to the conclusion that $\Delta\mathbf{K}^{p,j}$ is the unique member of the set $\mathcal{K}^p$. This (unique) member is given by equation (18).

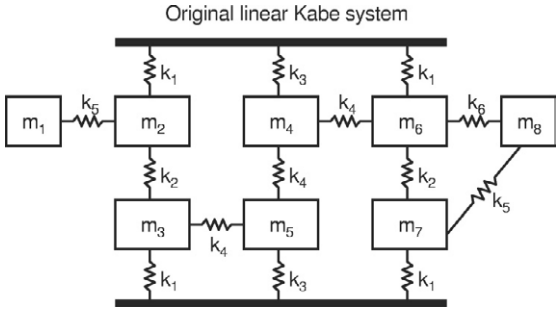

Figure 1. Kabe's problem [40].

The conclusions of the proposition above may be used to determine $\Delta\mathbf{K}$, and thus identify the damage location and extent. To identify the damage *location*, only right eigenvectors are needed in GMRPT. However, to identify the damage *extent* using GMRPT, p of the n left eigenvectors of the system are needed as well. One way of obtaining the left eigenvectors from the right eigenvectors is to use the mass orthogonality property of the eigenvectors given by

$$\mathbf{U}_\mathrm{d}^\mathrm{T}\mathbf{M}\mathbf{V}_\mathrm{d} = \mathbf{I}, \qquad \text{so that } \mathbf{U}_\mathrm{d}^\mathrm{T} = \mathbf{V}_\mathrm{d}^{-1}\mathbf{M}^{-1}. \tag{25}$$

An approach based on equation (25) requires all n right eigenvectors of the system to be known in order to solve for the left ones. In many vibratory problems in structural dynamics and/or fluid-structure interactions, the system of interest is modeled accurately by a system of equations of motion which is large dimensional (i.e. n is very large). Recent techniques for reducing the complexity of these models employs reduced-order modeling [3–8, 11, 13, 18] based on approaches such as component mode synthesis and proper orthogonal decomposition. These techniques are applicable to both linear and nonlinear systems and usually provide a transformation from the high-dimensional space of displacements $\mathbf{w}$ (of size n) to a reduced-order space $\mathbf{q}$ (of size $r \ll n$) as $\mathbf{w} = \mathbf{P}\mathbf{q}$, where $\mathbf{P}$ is a $n \times r$ matrix. Next, the equations of motion are expressed in the reduced-order space. For example, equation (3) successively becomes

$$\begin{gathered}\mathbf{M}\mathbf{P}\ddot{\mathbf{q}} + \mathbf{D}\mathbf{P}\dot{\mathbf{q}} + \mathbf{K}\mathbf{P}\mathbf{q} = \mathbf{0},\\ \mathbf{P}^\mathrm{T}\mathbf{M}\mathbf{P}\ddot{\mathbf{q}} + \mathbf{P}^\mathrm{T}\mathbf{D}\mathbf{P}\dot{\mathbf{q}} + \mathbf{P}^\mathrm{T}\mathbf{K}\mathbf{P}\mathbf{q} = \mathbf{0},\\ \bar{\mathbf{M}}\ddot{\mathbf{q}} + \bar{\mathbf{D}}\dot{\mathbf{q}} + \bar{\mathbf{K}}\mathbf{q} = \mathbf{0}.\end{gathered} \tag{26}$$

The reduced-order equation of motion in equation (26) has a low order r. Hence, its r right eigenvectors may be measured much more easily than the n right eigenvectors of the original problem. Once the r reduced-order right eigenvectors are obtained, the r left eigenvectors $\mathbf{e}_i$ (for $i = 1, \ldots, r$) of the reduced-order model may be computed using a relation similar to equation (25) by using the reduced-order mass matrix $\bar{\mathbf{M}}$. Next, the r most dominant full-size left eigenvectors are obtained as $\mathbf{u}_{\mathrm{d}i} = \mathbf{P}\mathbf{e}_i$, for $i = 1, \ldots, r$.

3. Examples of implementation of the proposed approach

To demonstrate its characteristics, this methodology was applied to an eight degree of freedom mass–spring system (Kabe system [38–41]), shown in figure 1. The parameter

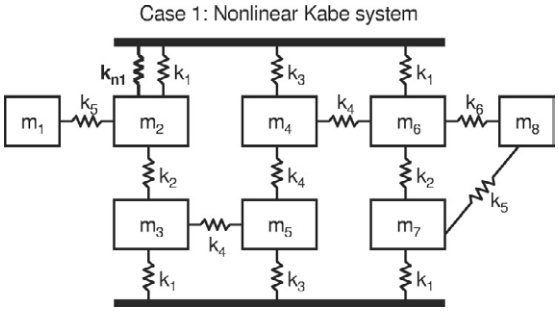

Figure 2. Kabe's problem [40] with addition of a nonlinear spring between mass two and ground.

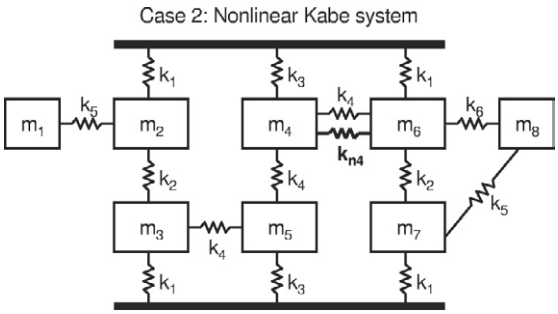

Figure 3. Kabe's problem [40] with addition of a nonlinear spring between mass four and mass six.

values are $m_1 = 0.001$, $m_8 = 0.002$, $m_j = 1$ for $j = 2, \ldots, 7$, $k_1 = 1000$, $k_2 = 10$, $k_3 = 900$, $k_4 = 100$, $k_5 = 1.5$, and $k_6 = 2$. First, the linear system was modeled, and then numerical tests were run using harmonic forcing at each of the masses to validate the GMRPT by comparison with previously published results [40]. Next, three nonlinear mass spring systems based on the Kabe system were created. The methodology was applied to each of the nonlinear systems, and numerical tests were conducted.

Kabe's problem shown in figure 1 is generalized into a nonlinear mass spring system in three cases. In each of the cases, the nonlinear springs are of the form $k_{ni}\Delta x^3$, where k_{ni} is the nonlinear spring stiffness, and Δx represents the distance the nonlinear spring is stretched. The first case consists of one nonlinear spring being added between mass two and ground as shown in figure 2 ($k_{n1} = k_1 = 1000$). The second case consists of one nonlinear spring being added between masses four and six as shown in figure 3 ($k_{n4} = k_4 = 100$). The third and last case consists of 12 nonlinear springs added between the masses and ground, as is illustrated in figure 4. The parameter values are $k_{n1} = 1000$, $k_{n2} = 10$, $k_{n3} = 900$, and $k_{n4} = 100$.

3.1. Case 1: methodology

This case consists of the addition of one nonlinear spring attached from mass two to ground as shown in figure 2. The nonlinear system equations are the same as the linear ones with the exception of the added term in the second degree of freedom and the augmented equation.

The added term in the second degree of freedom of the linear equation is $k_{2ng}y$, where k_{2ng} is the nonlinear spring

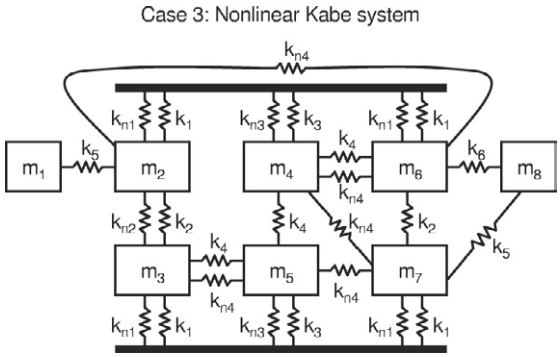

Figure 4. Kabe's problem [40] with addition of 12 nonlinear springs connecting masses to each other and ground.

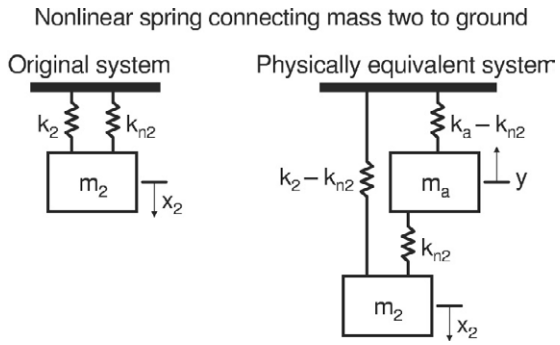

Figure 5. Physical equivalence of the augmentation for a nonlinear spring connecting a mass to ground.

stiffness that connects mass two to ground and $y = x_2^3$ (with x_2 being the displacement of mass two from its equilibrium). The augmented equation may be expressed as

$$\ddot{y} + k_{2ng}x_2 + 2k_{2ng}y = h(t). \tag{27}$$

A physical representation of the above system equation is demonstrated in figure 5, which illustrates how the use of an additional mass moving in a specified manner (i.e. $y = x_2^3$) in conjunction with linear springs can be used to account for the nonlinear spring. The additional mass results in an additional degree of freedom, which corresponds to the augmented equation for $h(t)$ given above.

3.2. Case 2: methodology

This case consists of a nonlinear spring attached between masses four and six, which results in a slightly more complicated model then the first (above) as shown in figure 3. The nonlinear system equations are again similar to the linear ones with the exception of the added term to the fourth and sixth degrees of freedom and the augmented equation.

The term $k_{4n6}y$ is added to the fourth degree of freedom equation, and it is subtracted from the sixth degree of freedom equation. The nonlinear spring stiffness is denoted by k_{4n6}, while the stretching of the nonlinear spring is $y = (x_4 - x_6)^3$. The augmented equation may be expressed as

$$\ddot{y} + k_{4n6}x_4 - k_{4n6}x_6 + 2k_{4n6}y = h(t). \tag{28}$$

The physical realization of the above system is demonstrated in figure 6. As in the case where the mass is connected with a nonlinear spring to the ground, the system can be physically represented by adding a mass and several springs to the system.

3.3. Case 3: methodology

This case consists of 12 nonlinear springs being added to the linear mass spring system as shown in figure 12. Each degree of freedom is modified in the same manner as done in the previous two sections. The following augmented equations are obtained:

$$
\begin{aligned}
&\ddot{y}_1 + k_{2ng}x_2 + 2k_{2ng}y_1 = h_1(t)\\
&\quad \text{where } y_1 = x_2^3,\\
&\ddot{y}_2 + k_{4n6}x_4 - k_{4n6}x_6 + 2k_{4n6}y_2 = h_2(t)\\
&\quad \text{where } y_2 = (x_4 - x_6)^3,\\
&\ddot{y}_3 + k_{5n7}x_5 - k_{5n7}x_7 + 2k_{5n7}y_3 = h_3(t)\\
&\quad \text{where } y_3 = (x_5 - x_7)^3,\\
&\ddot{y}_4 + k_{3ng}x_3 + 2k_{3ng}y_4 = h_4(t)\\
&\quad \text{where } y_4 = x_3^3,\\
&\ddot{y}_5 + k_{2n3}x_2 - k_{2n3}x_3 + 2k_{2n3}y_5 = h_5(t)\\
&\quad \text{where } y_5 = (x_2 - x_3)^3,\\
&\ddot{y}_6 + k_{6ng}x_6 + 2k_{6ng}y_6 = h_6(t)\\
&\quad \text{where } y_6 = x_6^3,\\
&\ddot{y}_7 + k_{4n7}x_4 - k_{4n7}x_7 + 2k_{4n7}y_7 = h_7(t)\\
&\quad \text{where } y_7 = (x_4 - x_7)^3,\\
&\ddot{y}_8 + k_{5ng}x_5 + 2k_{5ng}y_8 = h_8(t)\\
&\quad \text{where } y_8 = x_5^3,\\
&\ddot{y}_9 + k_{4ng}x_4 + 2k_{4ng}y_9 = h_9(t)\\
&\quad \text{where } y_9 = x_4^3,\\
&\ddot{y_{10}} + k_{7ng}x_7 + 2k_{7ng}y_{10} = h_{10}(t)\\
&\quad \text{where } y_{10} = x_7^3,\\
&\ddot{y_{11}} + k_{3n5}x_3 - k_{3n5}x_5 + 2k_{3n5}y_{11} = h_{11}(t)\\
&\quad \text{where } y_{11} = (x_3 - x_5)^3,\\
&\ddot{y_{12}} + k_{2n6}x_2 - k_{2n6}x_6 + 2k_{2n6}y_{12} = h_{12}(t)\\
&\quad \text{where } y_{12} = (x_2 - x_6)^3.
\end{aligned}
\tag{29}
$$

The stiffnesses of the nonlinear springs are denoted by an n in the subscript (i.e. k_{inj}).

4. Numerical results

To implement the methodology presented, a numerical simulation of the Kabe system was performed. The matrices **M**, **K** and **N** were obtained for the selected system, and each mass was forced harmonically. The vector of displacements $\mathbf{x}(t)$ was calculated by standard time integration, while $\mathbf{y}(t)$ and $\mathbf{h}(t)$ were calculated based on their relation to $\mathbf{x}(t)$. DSPI was employed for the augmented system to determine the eigenvalues and eigenvectors of the augmented matrices by using the time series for $\mathbf{x}(t)$, $\mathbf{g}(t)$, $\mathbf{y}(t)$ and $\mathbf{h}(t)$. Next, GMRPT was used to determine the damage location and extent by using the modal data provided by DSPI. Reduced-order modeling was not needed for this system since it only has eight linear degrees of freedom. Various damage scenarios were investigated using this approach for the three cases considered.

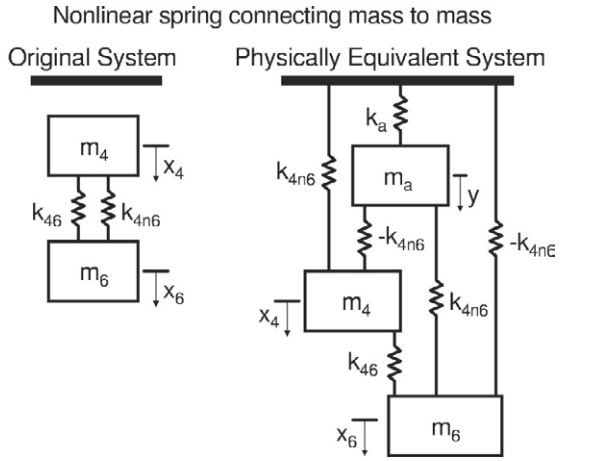

Figure 6. Physical equivalence of the augmentation for a nonlinear spring connecting a mass to another mass.

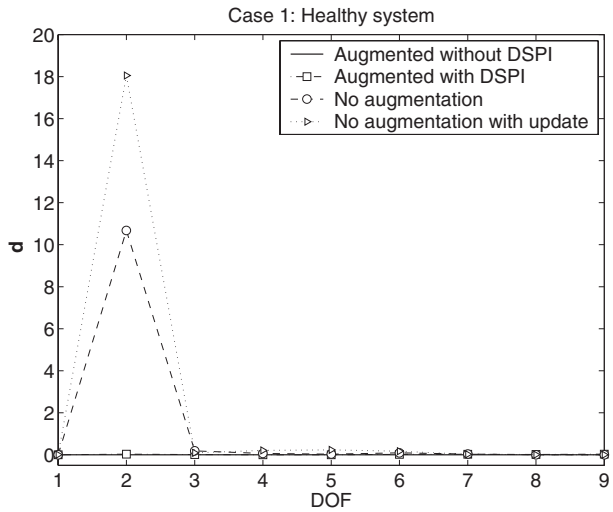

Figure 7. Results of the damage location algorithm applied to a healthy unaugmented nonlinear system and a healthy augmented nonlinear system for case 1.

4.1. Case 1: numerical results

In this section, two key characteristics of the nonlinear damage detection approach are discussed for a system with a nonlinear spring connected to the ground. First, the effect of the augmentation is discussed. Next, the relationship between MRPT and GMRPT is explored.

The effect of the nonlinearity on the healthy system can be seen in figure 7. The plot shows the damage location

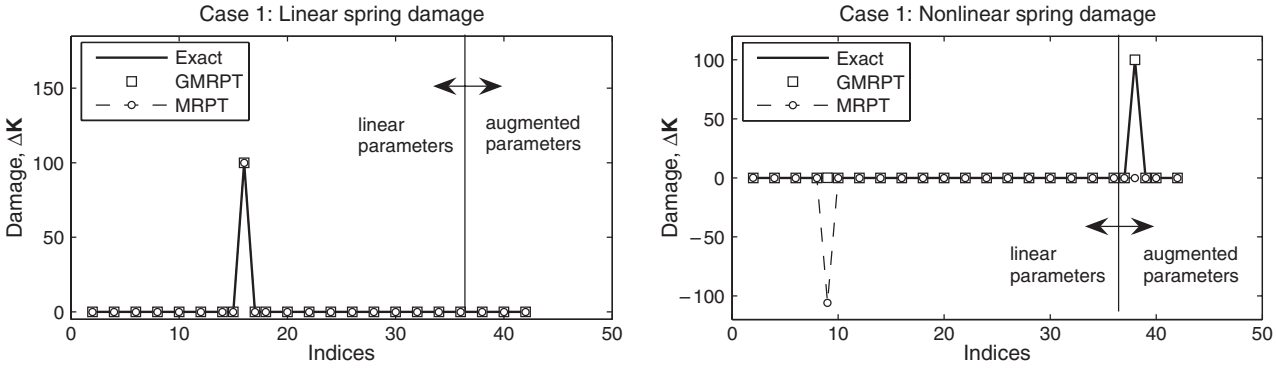

Figure 8. A comparison of results obtained for case 1 using GMRPT and MRPT for damage in a linear spring (left) and a nonlinear spring (right).

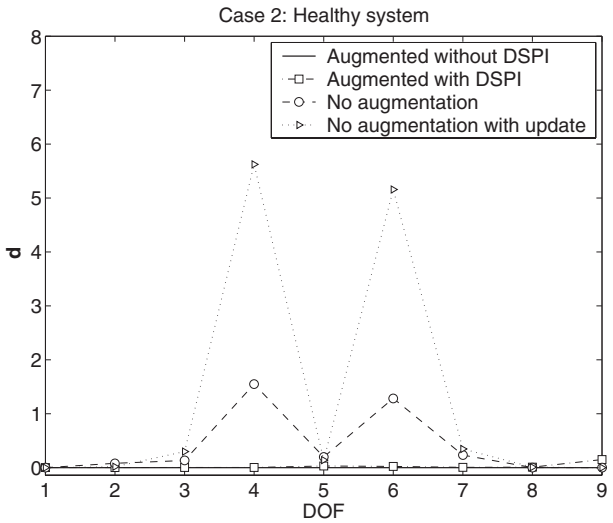

Figure 9. Results of the damage location algorithm applied to a healthy unaugmented nonlinear system and a healthy augmented nonlinear system for case 2.

obtained using equation (9) for four different approaches. The first approach (augmented without DSPI) uses an augmented system and a calculation where the *exact* eigenvalues and eigenvectors are used. This accurately predicts that no damage is present in any of the degrees of freedom. The second approach (augmented with DSPI) uses an augmented system and a calculation where DSPI is used to obtain eigenvalues and eigenvectors. These results show a very good estimate, with nearly zero damage predicted by GMRPT (as expected for a healthy system). In contrast, the next approach (no augmentation) uses DSPI to obtain the eigenvalues and eigenvectors also, but the system is modeled as the original linear system even though there is a nonlinear spring connecting mass two to ground. The results show that damage is erroneously predicted by the linear MRPT in the second degree of freedom, the location of the nonlinear spring.

The erroneous predictions of the linear MRPT are not alleviated by matrix updating. To show that, the stiffness matrix was updated with the damage predicted using MRPT and the forcing $\mathbf{g}(t)$ was slightly altered to simulate a change in forcing with time. The results are shown in figure 7 where the last approach (no augmentation with update) used DSPI with the updated linear model. This approach shows that the linear model is inaccurate when used to model a nonlinear system, despite matrix updating, because damage is still erroneously predicted at the degree of freedom that contains the nonlinearity.

MRPT is a subset of GMRPT, and detects damage in systems with symmetric damage. Hence, when the damage to a system is solely in its linear components, then both GMRPT and MRPT are accurate since the linear damage results in symmetric damage matrices, which result in $\mathbf{v}_{di} = \mathbf{u}_{di}$. Figure 8 presents element by element the values of the stiffness perturbation matrices ($\Delta\mathbf{K}$) obtained using MRPT and separately GMRPT (and using exact eigenvalues and eigenvectors of the augmented system). The x-axes in each plot represent the indices of a column vector obtained from storing the upper triangular portion of the perturbation stiffness matrix ($\Delta\mathbf{K}$) into a column vector. The linear and augmented parts of the matrix are demarcated by a line in the figure. The y-axes in the plots represent the entries of the difference between the original and updated stiffness matrices, $\Delta\mathbf{K}$. The left plot in figure 8 is the scenario where the linear spring connecting mass three to ground is reduced from a healthy value of 1000 to 900. Since the damage is linear, both MRPT and GMRPT predict accurately the exact damage of 100. The right plot in figure 8 is the scenario where the nonlinear spring is reduced from a healthy value of 1000 to 900. GMRPT is able to predict accurately the exact damage of 100, while MRPT incorrectly predicts damage in the linear spring that connects mass two to ground.

4.2. Case 2: numerical results

This section explores the same characteristics of the nonlinear damage detection approach as in case 1, except that the nonlinear spring connects two masses here instead of a mass and ground.

The effect of the nonlinearity on the healthy system can be discerned when comparing the approaches presented in figure 9. The plot shows the damage location obtained using equation (9) for four different approaches. These four approaches are the same as the ones in figure 7. The results in figure 9 show that damage is erroneously predicted by

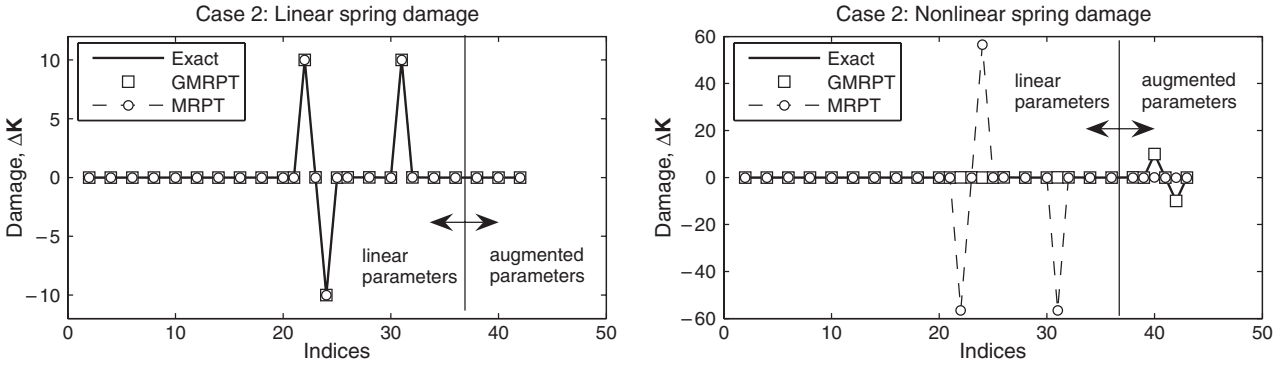

Figure 10. A comparison of results obtained for case 2 using GMRPT and MRPT for damage in a linear spring (left) and a nonlinear spring (right).

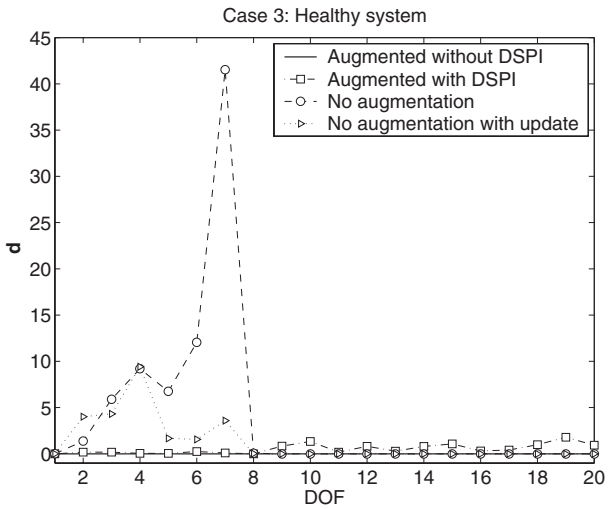

Figure 11. Results of the damage location algorithm applied to a healthy unaugmented nonlinear system and a healthy augmented nonlinear system for case 3.

MRPT in both degrees of freedom that the nonlinear spring affects for the approach with no augmentation. Also, the damage continues to be erroneously predicted by MRPT despite updating the stiffness matrix. In contrast, for the approach with the augmentation and exact eigenvalues and eigenvectors, zero damage is again accurately predicted by the proposed technique. Finally, the approach with the augmentation coupled with DSPI predicts low damage. This damage is negligible and is due to small inaccuracies in solving the eigenvalue problem by DSPI.

Figure 10 shows results which further explore the relationship between MRPT and GMRPT. An element by element plot of the stiffness perturbation matrices ($\Delta\mathbf{K}$) obtained using MRPT and separately GMRPT are shown. The left plot in figure 10 is the scenario where the linear spring connecting mass four to mass six is reduced from a healthy value of 100 to 90. Since the damage is linear, both MRPT and GMRPT predict accurately the exact damage of 10. The right plot in figure 10 is the scenario where the nonlinear spring is reduced from a healthy value of 100 to 90. GMRPT is able to predict accurately the exact damage of 10, while MRPT incorrectly predicts damage in the linear spring that connects mass four and mass six.

4.3. Case 3: numerical results

In this section, the characteristics of the proposed approach are demonstrated, and a discussion of the influence of noise is presented.

The effects of the nonlinearity on the healthy system can be discerned by comparing the cases presented in figure 11. The plot shows the damage location obtained by using equation (9) for four different approaches. These four approaches are the same as the ones in figures 7 and 9. The results in figure 11 show that damage is erroneously predicted by MRPT in all the linear degrees of freedom, except for one and eight (which are the two masses that do not have nonlinear springs attached to them). After updating, the erroneous damage does happen to be reduced, but there is still a significant extent of damage being inaccurately predicted by MRPT. For the approach where the augmentation is used with exact eigenvalues and eigenvectors, zero damage is accurately predicted by GMRPT. Finally, the approach with the augmentation coupled with DSPI predicts low damage, mainly in the augmented degrees of freedom, due to small inaccuracies in solving the eigenvalue problem by DSPI.

Next, one may further explore the relationship between MRPT and GMRPT. Figure 12 presents an element by element plot of the stiffness perturbation matrices obtained using MRPT and separately GMRPT. In this calculation, 1% random eigenvector noise and 0.1% random eigenvalue noise was added. The average damage values were calculated for each index, and standard deviation error bars are plotted for 100 separate calculations. The left plot in figure 12 is the scenario where the linear spring connecting mass four to mass six is reduced from a healthy value of 100 to 50, and the linear spring connecting mass three to ground is reduced from 1000 to 900. Since the damage is linear, both MRPT and GMRPT predict similar values with average values within 7% and 3%, respectively, of the exact damages. The right plot in figure 12 is the scenario where the nonlinear spring connecting mass three to five is reduced from a healthy value of 100 to 50, and the nonlinear spring connecting mass seven to ground is reduced from a healthy value of 1000 to 900. GMRPT is able to predict the damage within 1% of the exact damages, while MRPT incorrectly predicts that damage is present in the linear springs that connect mass three to mass five, and mass seven to ground.

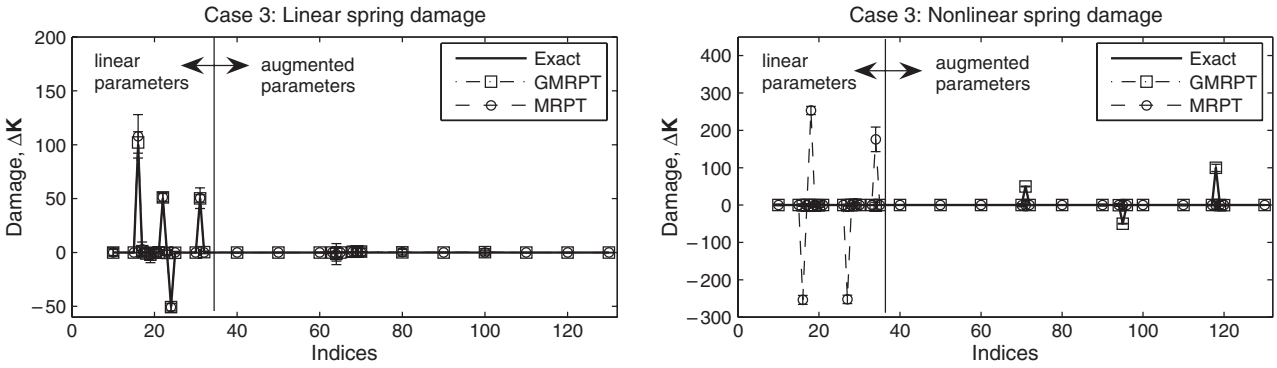

Figure 12. A comparison of results obtained for case 3 using GMRPT and MRPT for simultaneous damage in several linear springs (left) and several nonlinear springs (right) with 1% random eigenvector noise and 0.1% random eigenvalue noise.

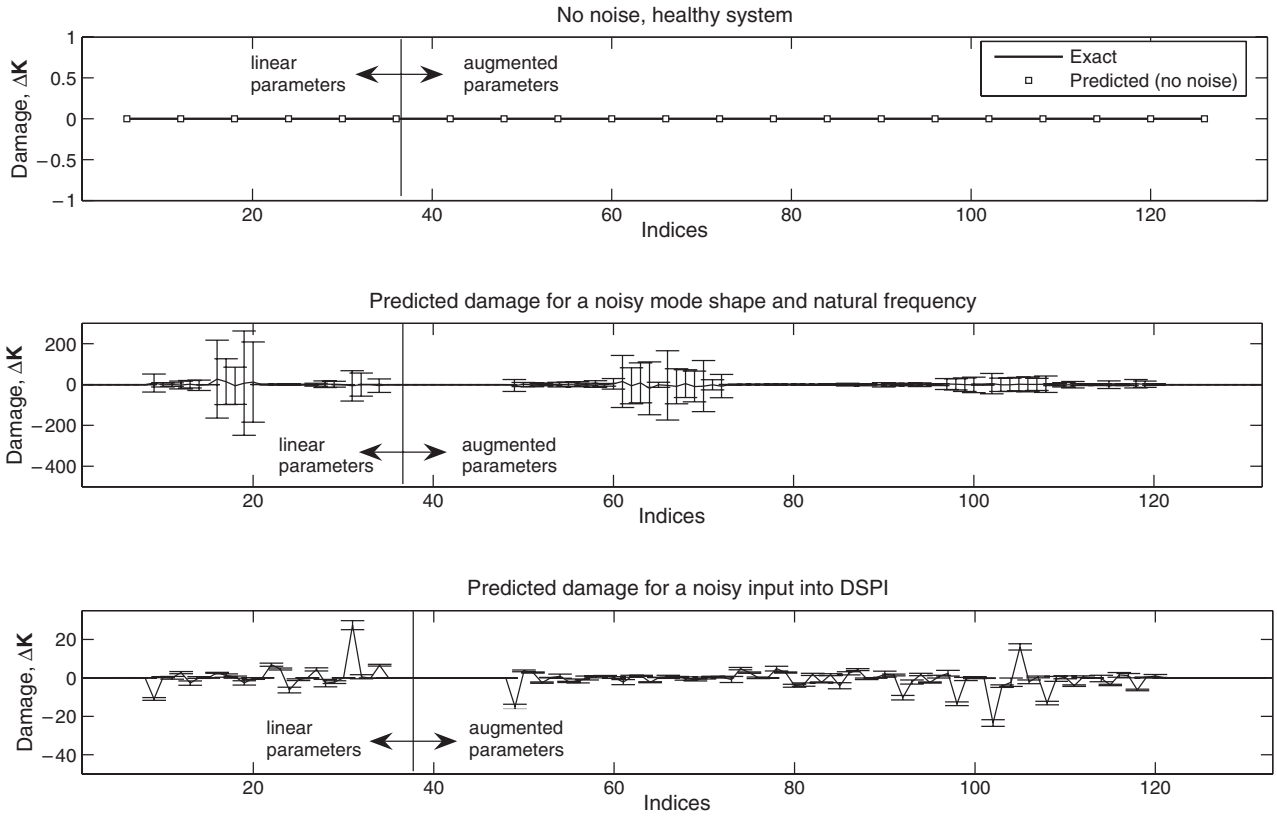

Figure 13. Predicted damage in healthy system for a case of no noise (top), 1% random eigenvector noise and 0.1% random eigenvalue noise (center), and ±0.0001 random noise input into DSPI (bottom).

To examine further the sensitivity of the proposed method to measurement noise, three scenarios are explored: (i) a scenario with no random noise, (ii) a scenario where noise is present in the measured eigenvectors and eigenvalues, and (iii) a scenario where noise is present in the measurements of $\mathbf{x}(t)$ (which is used by DSPI). An examination of the matrix $\Delta\mathbf{K}$ for a healthy system is shown in figure 13. The exact value of $\Delta\mathbf{K}$ is precisely zero since there is no damage. The plot on the top shows that the proposed method predicts the exact damage for the scenario of no noise. The other two plots represent scenarios with random measurement noise. The average damage values were calculated for each index, and standard deviation error bars are plotted for 100 separate calculations. The center plot in figure 13 shows damage predicted for 1% random eigenvector noise and 0.1% random eigenvalue noise. The average value for all indices is close to zero as it should be for a healthy system. The plot on the bottom of figure 13 presents the results for a scenario where ±0.0001 random noise was added to $\mathbf{x}(t)$, which was used by DSPI. The average values of the damages obtained in this case are larger than in the previous case, but they have much smaller standard deviations.

Figure 14 shows a scenario where a 10% damage is applied to a linear and a nonlinear spring. The linear spring connecting mass three to ground is reduced from 1000 to 900, and the nonlinear spring connecting mass four to ground is reduced

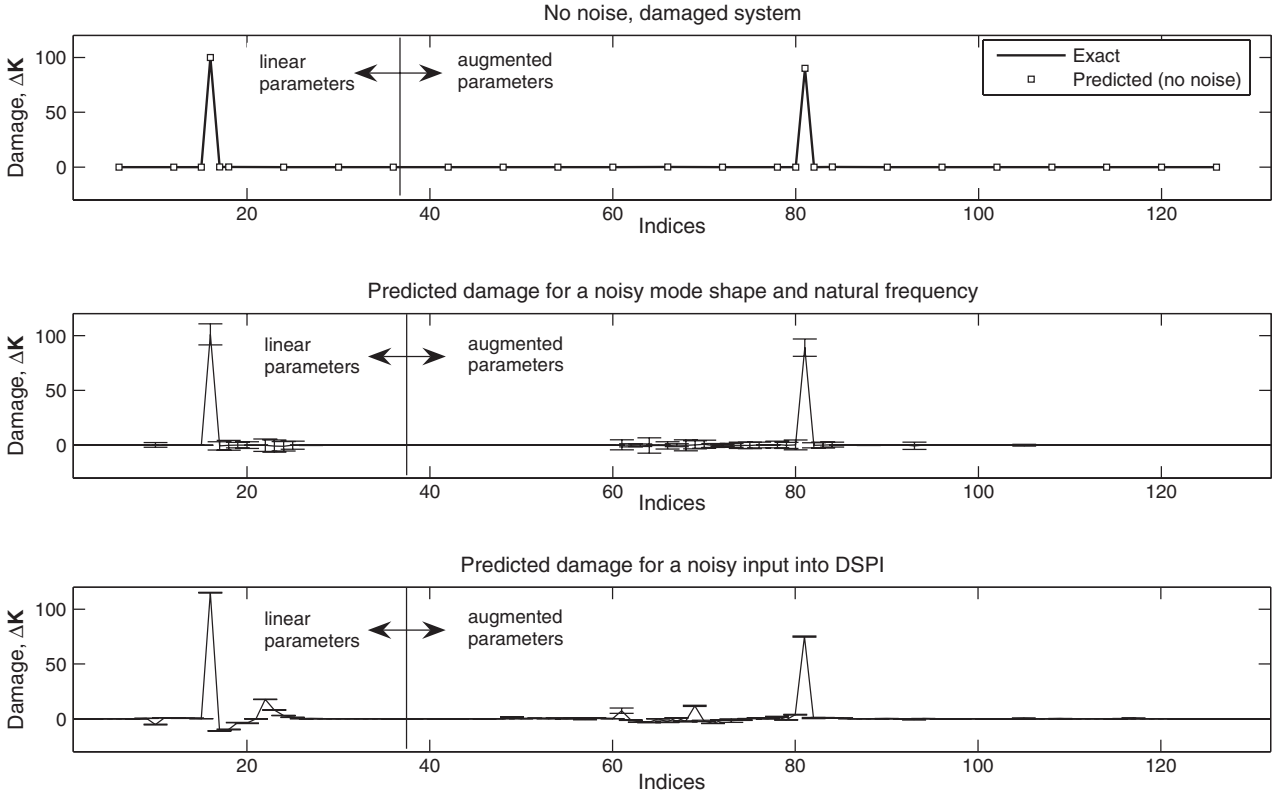

Figure 14. Predicted damage in a system with 10% damage in a linear and a nonlinear spring for a case of no noise (top), 1% random eigenvector noise and 0.1% random eigenvalue noise (center), and ±0.0001 random noise input into DSPI (bottom).

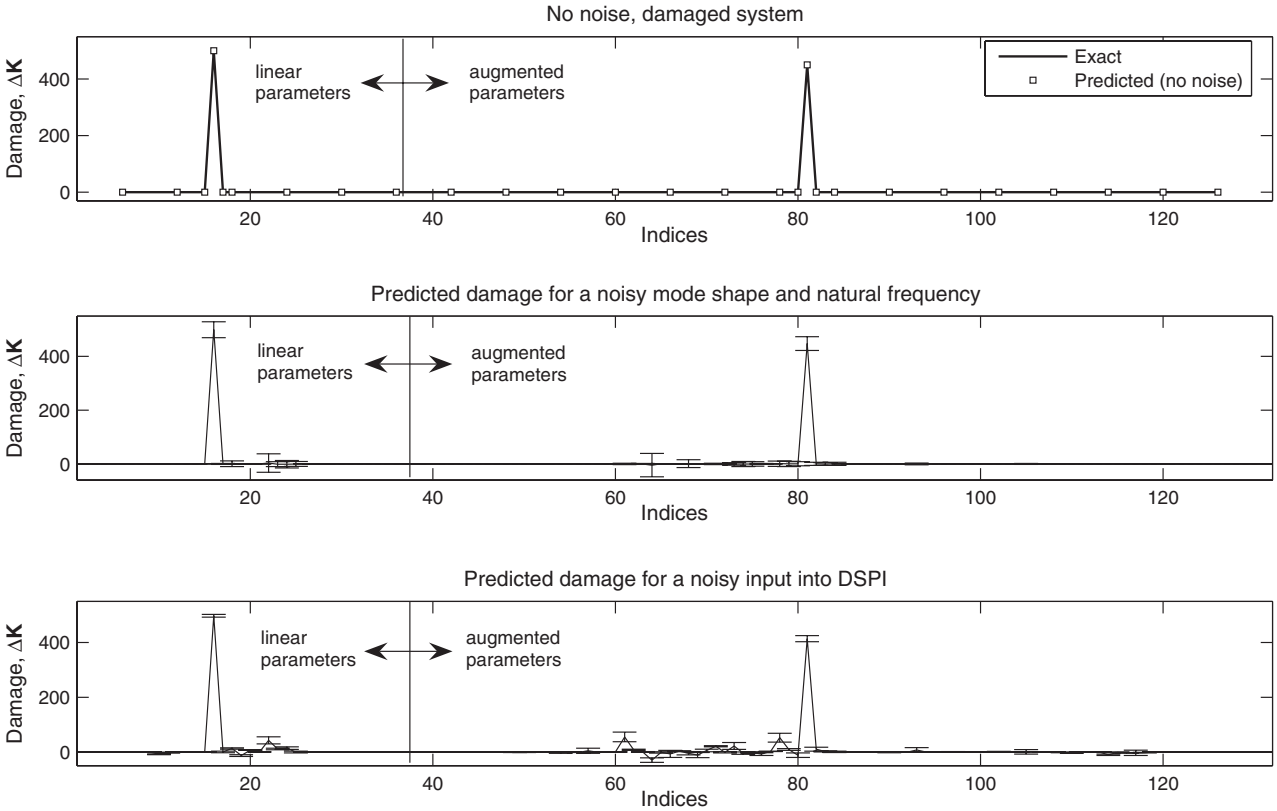

Figure 15. Predicted damage in a system with 50% damage in a linear and a nonlinear spring for a case of no noise (top), 5% random eigenvector noise and 1% random eigenvalue noise (center), and ±0.002 random noise input into DSPI (bottom).

from 900 to 810. The three plots are similar to figure 13, but here damage is present in the system. The plot on the top of figure 14 shows the exact damage being accurately predicted by GMRPT for the noise-free scenario. The plot in the center of figure 14 shows that the proposed approach can predict the damage extent within approximately 10% for the scenario with 1% eigenvector noise. Similarly, the plot on the bottom of figure 14 shows that the proposed approach can predict the damage extent within approximately 15% for the scenario with ± 0.0001 measurement noise.

Figure 15 shows a scenario where a 50% damage is applied to a linear and a nonlinear spring. The linear spring connecting mass three to ground is reduced from 1000 to 500, and the nonlinear spring connecting mass four to ground is reduced from 900 to 450. The three plots show results similar to figures 13 and 14, but here the damage applied is larger. The plot on the top of figure 15 shows the exact damage being predicted accurately by GMRPT for the noise-free scenario. The plot in the center shows that, with a level of 5% eigenvector noise, the average predicted value of the damage is within 1% of the actual damage. Finally, the plot on the bottom shows that, in the scenario where ± 0.002 random noise is present in the measurements, damage can be predicted within approximately 8% by the proposed technique.

The accuracy of GMRPT agrees well with results presented in the literature for MRPT [40]. In those studies, a much larger relative damage was applied (e.g. k_{78} was reduced by over 93%, from 1.5 to 0.1) and, as a result, MRPT was shown to be able to predict damage in the linear Kabe's problem with 5% eigenvector noise. The examples discussed here show that much smaller relative damages (of only 10% compared to 93.3%) can be detected if there is a lower eigenvector noise (of 1%).

5. Conclusions

A method to model nonlinear systems employing augmentation was presented, and a damage detection method was proposed. The proposed approach requires a discrete (e.g. finite element) model for the system. The nature of the augmentation requires the use of a modal analysis technique that has known but not prescribed forcing, such as DSPI. Once the eigenvalue problem was solved, the proposed approach was shown to predict accurately both the location as well as the extent of damage. A generalized minimal rank perturbation theory was presented. This method is able to address the issue of asymmetric damage caused by nonlinearities (and the augmentation).

The algorithms proposed have been demonstrated numerically for several different nonlinear mass–spring systems. The effectiveness of the proposed method was demonstrated, and the effects of measurement errors were presented.

Acknowledgments

The authors wish to acknowledge the National Science Foundation (CAREER program) and Professor Masayoshi Tomizuka and Dr Shih-ChiLiu (program directors) for the generous support of this work.

References

[1] Agbabian M S, Masri S F, Miller R F and Caughey T K 1990 System identification approach to detection of structural changes *ASCE J. Eng. Mech.* **117** 370–90
[2] Atalla M J and Inman D J 1998 On model updating using neural networks *Mech. Syst. Signal Process.* **12** 135–61
[3] Bazoune A, Khulief Y A, Stephen N G and Mohiuddin M A 2001 Dynamic response of spinning tapered Timoshenko beams using modal reduction *Finite Elem. Anal. Des.* **37** 199–219
[4] Bladh R, Castanier M P and Pierre C 1999 Reduced order modeling and vibration analysis of mistuned bladed disk assemblies with shrouds *J. Eng. Gas Turbines Power* **121** 515–22
[5] Bladh R, Castanier M P and Pierre C 2001 Component-mode-based reduced order modeling techniques for mistuned bladed disks—Part II: Application *J. Eng. Gas Turbines Power* **123** 100–8
[6] Castanier M P, Tan Y C and Pierre C 2001 Characteristic constraint modes for component mode synthesis *AIAA J.* **39** 1183–7
[7] Epureanu B I, Hall K C and Dowell E H 2000 Reduced order models of unsteady transonic viscous flows in turbomachinery *J. Fluids Struct.* **14** 1215–35
[8] Epureanu B I, Hall K C and Dowell E H 2001 Reduced order models of unsteady viscous flows in turbomachinery using viscous–inviscid coupling *J. Fluids Struct.* **15** 255–76
[9] Ewins D J 1984 *Modal Testing: Theory and Practice* (Taunton: Research Studies Press)
[10] Farrar C R, Doebling S W and Nix D A 2001 Vibration-based structural damage identification *Phil. Trans. R. Soc.* A **359** 131–49
[11] Farrell B F and Ioannou P J 2001 Accurate low-dimensional approximation of the linear dynamics of fluid flow *J. Atmos. Sci.* **58** 2771–89
[12] Feeny B F, Yuan C M and Cusumano J P 2001 Parametric identification of an experimental magneto-elastic oscillator *J. Sound Vib.* **247** 785–806
[13] Feldmann P and Freund R W 1995 Efficient linear circuit analysis by Padé approximation via the Lanczos process *IEEE Trans. Comput.-Aided Des. Integr. Circuits Syst.* **14** 639–49
[14] Gifford S J 1989 Volterra series analysis of nonlinear structures *PhD Thesis* Heriot–Watt University
[15] Heylen W and Sas P 1987 Review of model optimization techniques *Proc. 5th Int. Modal Analysis Conf. (London)* vol 2, pp 1172–82
[16] Ibrahim S R and Saafan A A 1987 Correlation of analysis in modeling and structures, assessment and review *Proc. 5th Int. Modal Analysis Conf. (London)* vol 2, pp 1651–60
[17] Juang J N and Pappa R S 1985 An eigensystem realisation algorithm for modal parameter identification and model reduction *J. Guid. Control Dyn.* **8** 620–7
[18] Kamon M, Wang F and White J 2000 Generating nearly optimally compact models from Krylov-subspace based reduced-order models *IEEE Trans. Circuits Syst.* II **47** 239–48
[19] Leuridan J 1984 Some direct parameter model identification methods applicable for multiple modal analysis *PhD Thesis* University of Cincinnati
[20] Levinson S J 1996 A Padé approach for eigenvalue identification in underwater acoustic normal mode computations *J. Acoust. Soc. Am.* **99** 831–5
[21] Ljung L 1999 *System Identification—Theory for the User* (New York: Prentice-Hall)
[22] Ma X, Azeez M F A and Vakakis A F 2000 Non-linear normal modes and non-parametric system identification of non-linear oscillators *Mech. Syst. Signal Process.* **14** 37–48
[23] Marwala T and Hunt H E M 1999 Fault identification using finite element models and neural networks *Mech. Syst. Signal Process.* **13** 475–90

[24] Masri S F, Miller R K, Saud A F and Caughey T K 1987 Identification of nonlinear vibrating structures: Part I: Formulation *J. Appl. Mech.* **109** 918–22
[25] Mirri D, Iuculano G, Filicori F, Pasini G G, Vannini G and Gualtieri G P 2002 A modified Volterra series approach for nonlinear dynamic systems modeling *IEEE Trans. Circuits Syst.* I **49** 1118–28
[26] Pandey A K and Biswas M 1994 Damage detection in structures using changes in flexibility *J. Sound Vib.* **169** 3–17
[27] Pesheck E, Pierre C and Shaw S W 2001 Accurate reduced-order models for a simple rotor blade model using nonlinear normal modes *Math. Comput. Modelling* **33** 1085–97
[28] Shaw S W and Pierre C 1993 Normal modes for non-linear vibratory systems *J. Sound Vib.* **164** 85–124
[29] Shong W and Zhang P Q 1988 MIMO ITD identifying technique for mini-computer *J. Univ. Sci. Technol. China* **18** 195–202
[30] Smyth A W, Masri S F, Chassiakos A G and Caughey T K 1999 On-line parametric identification of MDOF nonlinear hysteretic systems *ASCE J. Eng. Mech.* **125** 133–42
[31] Steiner W, Steindl A and Troger H 1995 Center manifold approach to the control of a tethered satellite system *Appl. Math. Comput.* **70** 315–27
[32] Vold H and Rocklin G T 1982 The numerical implementation of a multi-input modal estimation for mini-computers *Proc. 1st Int. Modal Analysis Conf. (Orlando, FL)* vol 1, pp 542–8
[33] Worden K and Tomlinson G R 2001 Nonlinearity in experimental modal analysis *Phil. Trans. R. Soc.* A **359** 113–30
[34] Xiao M Q and Basar T 2000 Center manifold of the viscous Moore–Greitzer PDE model *SIAM J. Appl. Math.* **61** 855–69
[35] Yang Q J, Zhang P Q, Li C Q and Wu X P 1994 A system theory approach to multi-input multi-output modal parameters identification methods *Mech. Syst. Signal Process.* **8** 159–74
[36] Zang C and Imregun M 2001 Structural damage detection using artificial neural networks and measured FRF data reduced via principal component projection *J. Sound Vib.* **242** 813–27
[37] Zhang P Q, Li C Q and Yang Q J 1989 Identification of structural modal parameters by ARMAV model method *J. Exp. Mech.* **4** 137–45
[38] Zimmerman D C 1999 Looking into the crystal ball: the continued need for multiple viewpoints in damage detection *Key Eng. Mater.: Damage Assessment Struct.* **167/168** 76–90
[39] Zimmerman D C 2000 Model validation and verification of large and complex space structures *Inverse Probl. Eng.* **8** 93–118
[40] Zimmerman D C and Kaouk M 1994 Structural damage detection using minimum rank update theory *ASME J. Vib. Acoust.* **116** 222–31
[41] Zimmerman D C and Simmermacher T 1995 Model correlation using multiple static load and vibration tests *AIAA J.* **33** 2182–8